Performance Evaluation of Solar Module with Emulator and DC Microgrid

Vijay Kumar Garg[1,2,‡] iD, Sudhir Sharma[3] iD

1 (Research Scholar) IKG Punjab Technical University, Jalandhar, India

2Department of Electrical Engineering, UIET, Kurukshetra University, Kurukshetra, India

3Department of Electrical Engineering, DAV Institute of Engineering and Technology, Jalandhar, India

(vkgarg.ee@gmail.com, Sudhir.abc@gmail.com)

‡ Vijay Kumar Garg; Corresponding author, Department of Electrical Engineering, UIET, Kurukshetra University, Kurukshetra, India, Email: vkgarg.ee@gmail.com

Abstract: Increasing energy demand, depletion in fossil fuels, and environmental constraints emphasize the development and research of renewable energy resources. Solar energy sources are abundant in nature and gaining acceptance worldwide to meet the energy demand. Solar modules' performance depends on various factors, and investigation using the real solar module is uneconomical and depends on time factors. In this paper, the performance of the solar module has been evaluated with a solar PV emulator (SPVE). The I-V and P-V characteristics are analyzed under various environmental conditions. Grid integrated DC microgrid hardware system comprising SPVE, battery energy storage system has been analyzed using LabVIEW interfaced GUI system. The effect of the duty ratio of buck converter has been investigated on the load line and power production, which further affects the power intake/export with the utility grid. MPPT controller helps in the optimized operation of the solar module. Therefore, variation of power output under manual sliding controller and MPPT controller has been analyzed. SPVE replicates the actual environmental effects, and research on various shortcomings of solar modules can be investigated to enhance their acceptance as solar integrated microgrid systems.

1. Introduction

Environmental concerns, increasing energy demand, and depletion of fossil fuels have inspired people to use renewable energy resources (RERs) like solar PV, wind energy, geothermal, biogas, etc. Globally, the renewable energy composition is increasing, and it will attain a level of 40% in total energy production up to 2050 [1]. India stands third in electricity production as well consumption. India is very rich in solar capacity, with approximately 300 clear sunny days. The Government of India (GOI) targets to achieve the generation of 175GW from RER with 100 GW from Solar PV, 60 GW of energy from wind power, 10 GW from Bioenergy, and 5GW from mini and micro-hydropower up to 2022.

Solar energy is utilized in various forms, and electricity is produced by various combinations of solar modules and solar thermal systems, which are further affected by various environmental constraints. Solar cell evolves from single/multi-crystalline silicon wafer technology, thin-film PV technologies such as Cadmium-Telluride, amorphous silicon/micromorph silicon, Copper Indium Selenide (CIS)/Copper Indium Gallium Diselenide (CIGS) to Concentrating PV (CPV) and organic PV cells [2]. The current-voltage (I-V) curve behaves like a non-linear curve, and power voltage (P-V) curves have maximum power point (MPP), which varies as per solar irradiation and temperature [3]. Electrical power fluctuates depending upon operating conditions and field factors like geographical location, irradiation level, ambient temperature, etc. [4]. The efficiency of the PV module decreases with various partial shading factors like building, wildlife, passing clouds, tree, snow. Due to this, PV modules receive variable irradiations, which further cause multiple peaks in their characteristics and give rise to the hotspot in the cell [5]–[7]. A bypass diode is connected across each module to minimize the effect of hot spots, which generates losses. There are various types of mismatch losses in PV systems like non-homogeneous characteristics of cells, manufacturing defects, doping ratio, aging, dirt deposition, varying temperature, and irradiance [8].

Real solar power system faces various challenges in coordination, voltage regulation, and transient stability, etc [9], [10]. Experimental validation of PV modules under

different working conditions is very rigorous, time-consuming, and depends on seasonal/environmental factors [11]. Solar PV Emulator (SPVE) emulates the characteristics and behavior of the solar module. A precise and experimental validation of the PV system can be performed with a Solar PV emulator [12], [13]. SPVE evolves from a mathematical model to real-time controllers. They can be classified as diode model approximation, converter-based model, real-time and hybrid converter [14]. The power converter plays a significant role in power extraction from solar modules [15], [16]. The emulator comprises three parts, i.e., PV model, control strategies, and power converter. The various PV models are electric circuit and interpolation, while direct calculation, look-up table, piecewise linear, neural and curve segment, etc., are implementation methods. Several control strategies like direct referring, hybrid, analog-based, partial shading, etc., are implemented to determine the operating point of the emulator. Finally, the actual I-V characteristics are obtained from non-power V-I characteristics of PV model by power converter such as a linear regulator, switched-mode power supply (SMPS), and programmable power supply [17].

In this paper, the characteristics of the PV module under various environmental factors have been analyzed using a laboratory-scale setup of the Solar PV Emulator (SPVE). The hardware implementation of SPVE in real-time with grid integrated DC microgrid is presented, and the effects of PV duty on power interchange are analyzed. Section 2 describes the mathematical modeling of the PV cell. The hardware model of the solar PV emulator and DC microgrid is presented in sections 3 and 4, respectively. In section 5, the experimental results of PV characteristics with SPVE and DC microgrid systems.

2. Mathematic Modelling of PV cell

PV cell produces power according to their manufacturing technique. A very low voltage is generated in the range of 0.5-0.8 volts. Therefore, the PV modules are connected in various combinations of series/parallel. In series, the overall voltage increases, while in parallel resultant current increases without change in voltage [18]. The single diode model/1D2R/five parameter model; two diode model/ 2D2R model/ eight parameter model and PV module are depicted in Figure 1 (a), (b) and (c) respectively. The double diode model is complex but gives accurate PV module characteristics under low irradiation, partial shading, and mono and polycrystalline silicon cells [17]. The circuit consists of a photoelectric

current (I_{PH}), diode current (I_D), shunt current (I_{SH}), shunt resistance (R_{SH}) to represent the leakage current and series resistance (R_S) resenting internal resistance of the cell, series branches (N_S) and parallel branches (N_P). The various voltage and current equations are as follow [17]–[19]. In the case of a single diode, Fig 1(a)

$$I_L = I_{PH} - I_D - I_{SH} \tag{1}$$

$$I_L = I_{PH} - I_o\left[exp\frac{q}{AkT}(V_L + I_L R_S) - 1\right] - \frac{V_L + I_L R_S}{R_{SH}} \tag{2}$$

where I_o is dark saturation current, T is operating temperature in kelvin(K), q is electron charge (1.602×10^{-19} C), k is Boltzmann constant (1.3806503×10^{-23} J/K), and A is diode ideality factor. In the case of two diode models, Fig 1(b)

$$I_L = I_{PH} - I_{o1}\left[exp\frac{q}{A_1 kT}(V_L + I_L R_S) - 1\right] - I_{o2}\left[exp\frac{q}{A_2 kT}(V_L + I_L R_S) - 1\right] - \frac{V_L + I_L R_S}{R_{SH}} \tag{3}$$

While, in the case of the PV module, Fig 1(c)

$$I_L = N_P I_{PH} - N_P I_o\left[exp\frac{q}{AkT}\left(\frac{V_L}{N_S} + I_L\frac{R_S}{N_P}\right) - 1\right] - \frac{\frac{N_P}{N_S}V_L + I_L R_S}{R_{SH}} \tag{4}$$

In the PV module, R_S becomes important, and R_{SH} approaches infinite, so efficiency is sensitive to small changes in R_S while not much effective by R_{SH}. In case, $N_S = N_P = 1$, the equation can be rewritten as

$$I = N_P I_{PH} - N_P I_o\left[exp\frac{q}{AkT}\left(\frac{V_L}{N_S} + I_L\frac{R_S}{N_P}\right) - 1\right] \tag{5}$$

The most simplified form is as

$$I = N_P I_{Ph} - N_P I_o\left[exp\left(\frac{qV_L}{N_S AkT}\right) - 1\right] \tag{6}$$

The I_{Ph} depends upon solar irradiation and temperature, which is given as

$$I_{PH} = [I_{sc} + K_I(T - T_{REF}]\frac{G}{G_N} \tag{7}$$

Where I_{SC} is short circuit current at 25°C and 1000W/m², short circuit current temperature coefficient K_I, T_{REF} as reference temperature, G is solar irradiation of cell, and G_N represents nominal solar irradiation in W/m². The saturation current varies with cell temperature and can be expressed as

$$I_o = I_{o,N}\left(\frac{T_{REF}}{T}\right)^3 exp\left[\frac{qE_G}{Ak}\left(\frac{1}{T_{REF}} - \frac{1}{T}\right)\right] \tag{8}$$
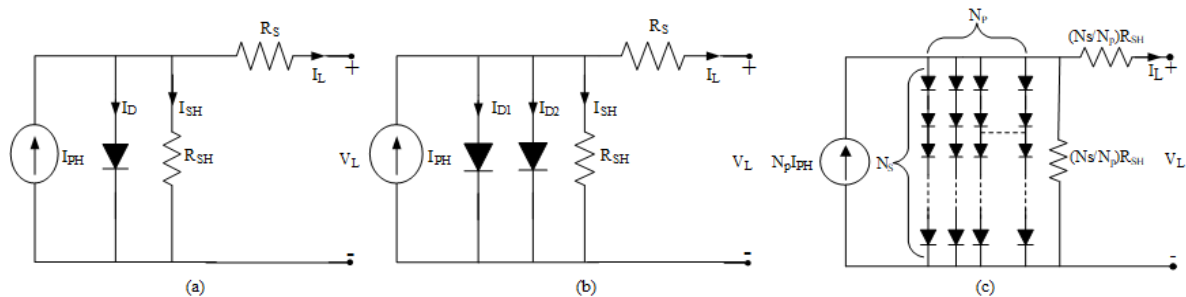

Fig 1. Different modes of solar PV module

Where $I_{o,\,N}$ is reverse saturation current at the reference temperature and solar radiation, E_G is bandgap energy of the semiconductor used for the cell. The ideality factor A depends upon the PV technology [18], given in Table 1.

Table 1. Ideality factor of various solar cells

Solar cell Technology	Ideality Factor
Silicon monocrystalline	1.20
Silicon-polycrystalline	1.30
Amorphous Silicon (a-Si):H	1.80
Amorphous Silicon (a-Si):H tandem	3.30
Amorphous Silicon (a-Si):H triple	5.0
Cadmium Telluride (CdTe)	1.50
Copper Indium Selenide (CIS)	1.50
Gallium arsenide (GaAs)	1.3.

3. PV emulators

The rise in penetration level of solar energy motivates the researcher to evaluate various characteristics of the solar PV system. Analysis of actual PV modules faces various environmental issues with irradiations, temperature, etc. Solar PV Emulator (SPVE) emulates the I-V, P-V characteristics of the real PV panel. The emulator should have the capability to interface with power electronics converters, change the operating point as per load change, replicate characteristics under changing environmental factors, partial shading, etc. A detailed analysis of PV emulators can be accessed in reference [14], [17].

The SPVE consists of SMPS, DC-DC converter, and a capacitor is shown in Fig. 2. The output of SMPS can vary from 0-48V and 0-21A. The buck converter covers the wide range of I-V characteristics of the PV emulator. The irradiation (W/m²) having four different channels and
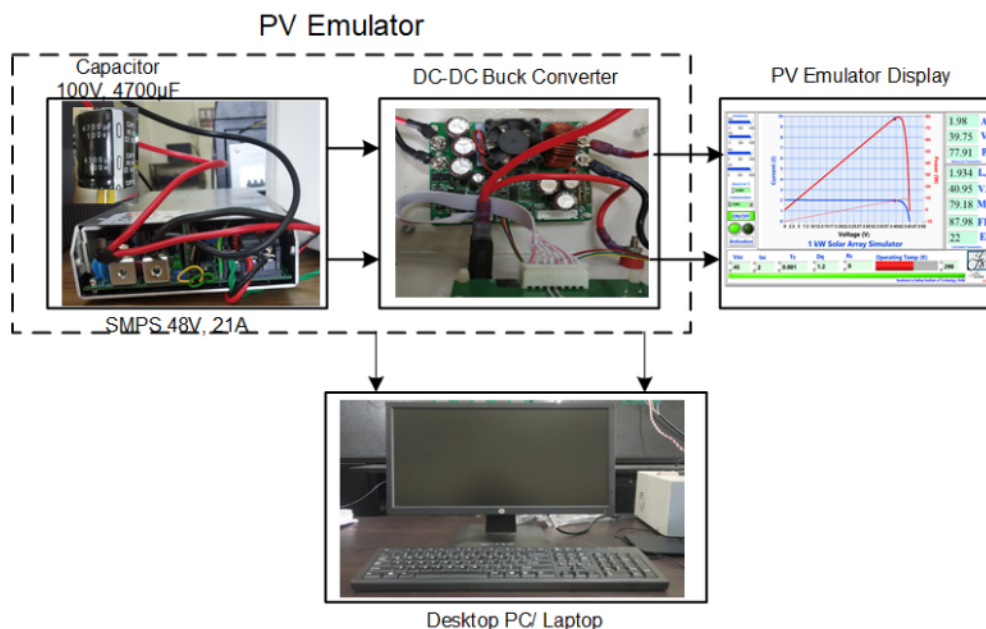

Fig. 2. PV Emulator control system

operating temperature (K) is given as input to the SPVE. The I-V and P-V characteristics can be obtained per module open-circuit voltage, $V_{OC,}$ and short circuit current, I_{SC}. The SPVE requires minimal size and self-protection ability under overload/short-circuit conditions. The characteristics of various solar cells can be reproduced under different atmospheric conditions.

4. Hardware implementation of SPVE with DC microgrid

Integration of renewable energy sources with the electricity grid improves the overall performance of the power system. A hardware model of grid integrated DC microgrid consisting of solar PV emulator and battery energy storage system is shown in Fig. 3. The output of SPVE is connected

to DC Link having a voltage range of 110-150V through a boost converter. The output voltage can be controlled by duty cycle; D. Pulse Width Modulation (PWM) system is used for controlling the pulses which are fed to the converter system as per duty cycle. Data acquisition has been performed through FPGA based NI-sbRIO-9607 (National Instruments) data card. It is connected to the primary system through CAT-5 or above LAN cable with RJ-45 gigabit ethernet port. The input and output operating signal range from 0-5V. All quantities are measured through various transducers and scaled in the operating range.

5. Results and discussion

The solar PV characteristics and integration of SPVE with DC microgrid have been analyzed in this section.
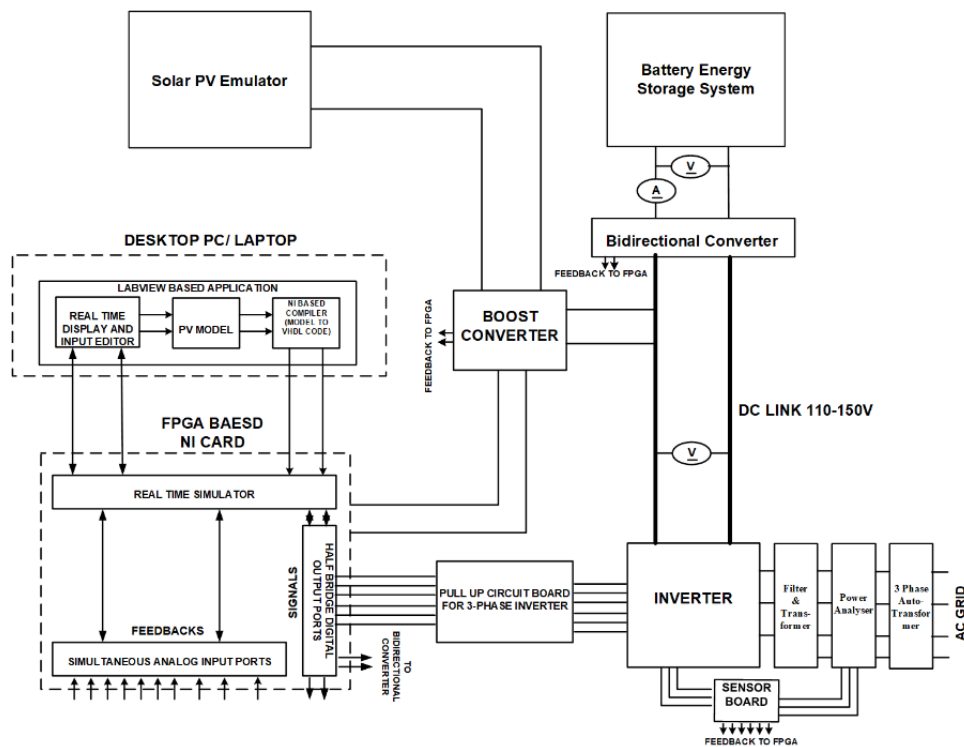
Fig. 3. Hardware model of SPVE with DC microgrid

5.1. PV characteristics with SPVE

The solar PV system characteristics are analyzed under various environmental conditions using SPVE. The PV module open-circuit voltage, V_{OC}, is considered as 45 Volts and the short circuit current, I_{SC} as 5 Amp.

The effect of variation in irradiation level from 500-1000 W/m^2 on the I-V and P-V characteristics are depicted in Fig. 4 and 5, respectively. The open-circuit voltage rises slightly, whereas linear variation in short circuit current. The output power of the module increases with an increase in solar intensity.

The partial shading affects the performance of the PV module. The maximum power obtained from the overall system reduces as compared to uniform irradiation conditions. In this investigation, four channels are operated at different irradiation levels. There will be uniform irradiation in condition A at all four channels, i.e., G1, G2, G3, and G4, which is 1000 W/m^2. In case B, G1, G2, G3, and G4 are at 1000, 900, 800, and 700 W/m^2, respectively, whereas in case C, irradiation level for four channels is at 1000, 800, 700, and 600 W/m^2, respectively. The I-V and P-V characteristics are depicted in Fig. 6 and 7, respectively. The maximum power point, form factor, and efficiency of the solar module decrease due to the partial shading.
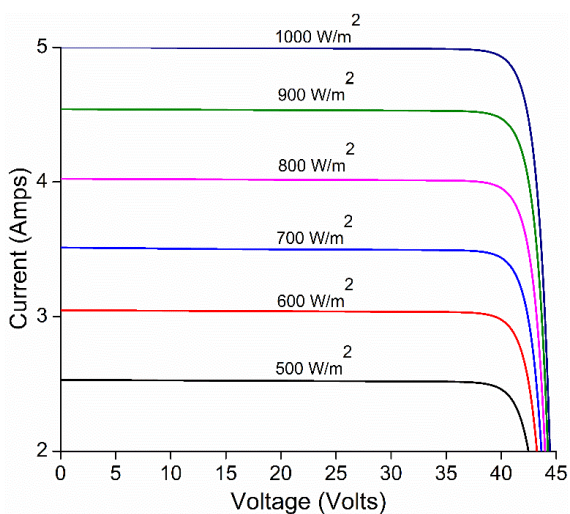

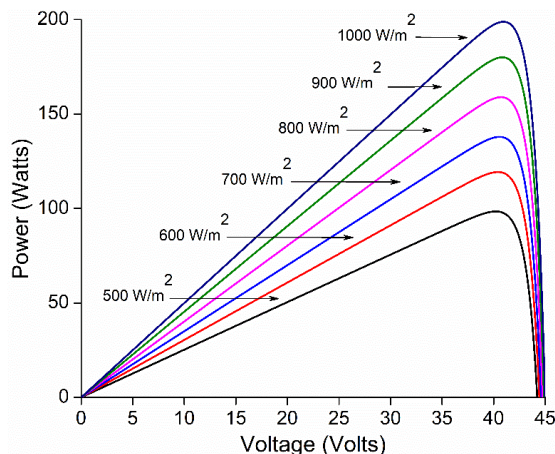**Fig. 4.** IV characteristics under different solar irradiation
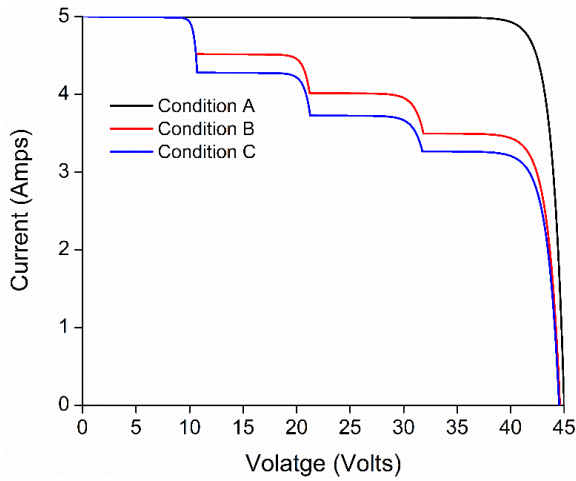

Fig. 5. PV characteristics under different solar irradiation

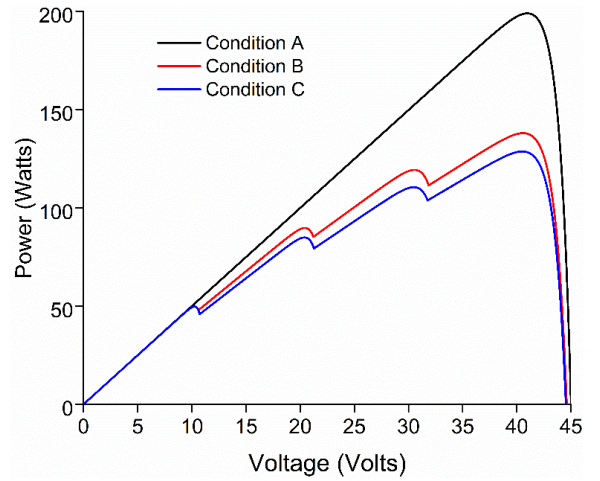**Fig. 6.** IV characteristics under partial shading

Fig. 7. PV characteristics under partial shading

Fig.8. Hardware model of DC microgrid

1556

5.2. Hardware results

The hardware system comprising various components is shown in Fig. 8. The solar PV emulator output is connected with DC Link through a boost converter. The DC microgrid is connected with the utility grid through a three-phase autotransformer. The solar panel parameters such as V_{OC} and I_{SC} have been considered as 45V and 8A. Uniform irradiation of 1000W/m² and temperature of 25°C are considered. The hardware model is run through LabVIEW based GUI platform, as shown in Fig. 9 (A). The V_{DC} Ref is set at 120V. As the inverter is switched ON, the DC microgrid line voltage is

synchronized with reference DC voltage. The DC-DC buck converter The PV duty is varied from 0 to 0.9 through PWM. As boost converter duty, i.e., called PV duty in this hardware model, increases from 0 to 0.45, the hardware system consumes the power from the grid. When the PV duty rises to 0.5, the SPVE starts exporting the power to the grid. At 0.7, it reaches the maximum, as shown in figure 9 (C). After further variation in boost converter duty, the load line shifts to the left of P-V characteristics, and there is a fall in output power of the SPVE, as shown in figure 9 (D-G). The complete I-V, P-V characteristics are shown in figure 9 (H).
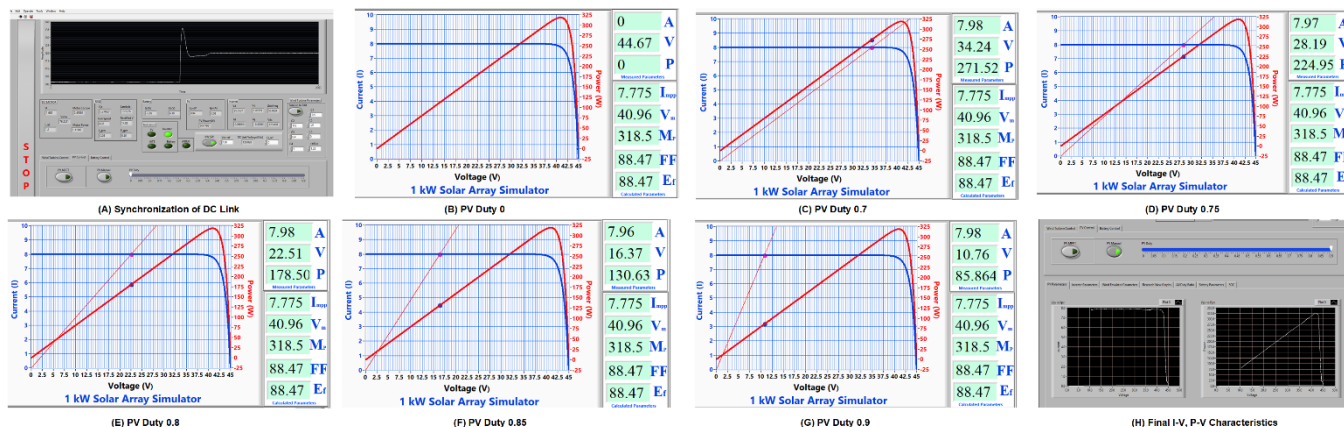

Fig. 9. Variation of PV characteristics with duty ratio of converter
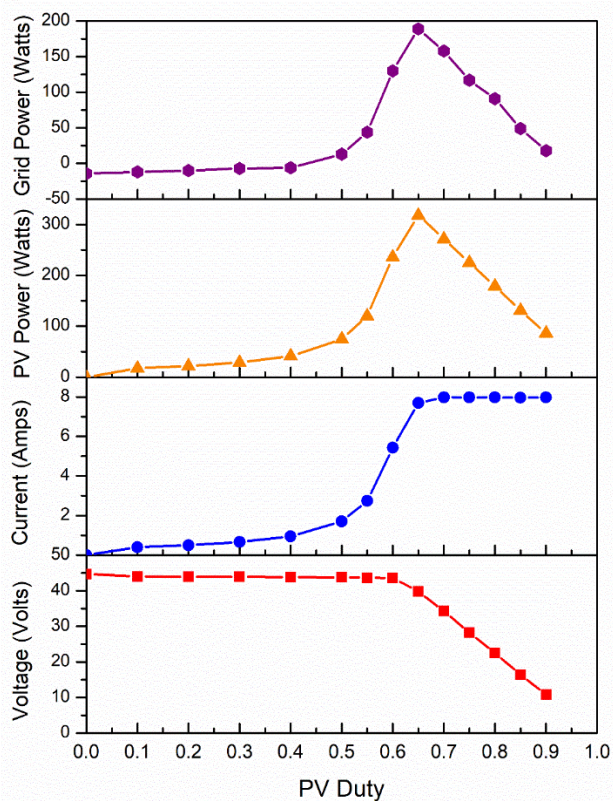

Fig. 10. Variation of various parameters with PV duty
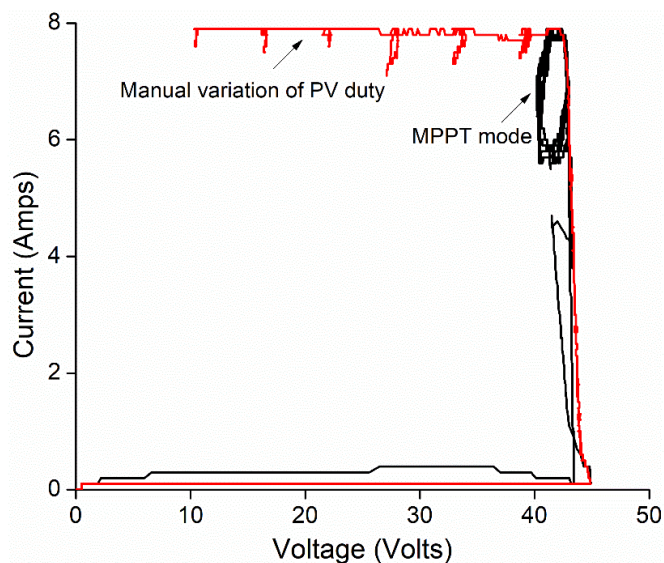
Fig. 11. I-V characteristics under MPPT

The variation of grid interfaced power, power produced by solar PV emulator, $I_{SC,}$ and V_{OC} variation with boost converter duty is shown in Fig. 10. The hardware model uses Perturb & Observation (P&O) method for MPPT. The MPPT can be varied manually by sliding the PV duty and automatic by the MPPT controller. The I-V and P-V characteristics under both modes of MPPT are depicted in Fig. 11 and 12, respectively. In MPPT mode, when it attains maximum value,

Table 2. Variation of various parameters with PV duty and module current

S. No.	PV Duty	I_{PV} (Amps)	V_{PV} (Volts)	PV Power (Watts)	Grid Power (Watts)	Maximum I_{SC} (Amps)
1	0	0008	45	0	-16	2
2	0.1	0.4	43.83	17.53	-14	2
3	0.2	0.49	43.75	21.875	-12	2
4	0.3	0.65	43.68	28.39	-10	2
5	0.4	0.93	43.63	40.575	-9	2
6	0.45	1.2	43.61	52.33	-1	2
7	0.5	1.63	43.09	70.2	10	2
8	0.55	1.98	39.57	78	17	2
9	0.55	2.55	42.87	108.89	36	3
10	0.6	2.98	38.53	114.49	48	3
11	0.6	3.94	40.57	162	72	4
12	0.6	4.7	42.17	195	90	5
13	0.65	4.98	37.05	184	98	5
14	0.65	5.98	38.23	228.9	126	6
15	0.65	6.98	39.44	273	159	7
16	0.65	7.98	40	320	183	8
17	0.65	8.98	41	362	217	9
18	0.65	9.98	42	411	252	10
19	0.65	10.5	41.7	433	272	11
20	0.7	10.98	36.04	395.37	243	11
21	0.7	11.98	36.5	435	272	12
22	0.75	11.98	30.67	367	216	12
23	0.8	11.98	24.45	292	155	12
24	0.8	12.98	24.94	323	173	13
25	0.8	13.97	25.34	355	189	14
26	0.8	14.95	25.84	387.27	206	15
27	0.8	15.97	26.4	418.01	219	16
28	0.8	16.97	26.7	452	240	17
29	0.8	17.97	27.11	484	254	18
30	0.8	18.98	27.56	521	276	19
31	0.8	19.97	27.73	555	294	20

it moves backward and forwards near maximum value, while in manual mode, the current remains the same, voltage and power decreases with further increase in converter duty. Experimental variation of various parameters with buck converter duty and module short circuit current rating is tabulated in Table 2. The module is taken with a V_{OC} of 45V, and I_{SC} is initialized from 2A. The PV buck converter duty is increased from 0 and slightly raised. When the PV current attains maximum value w.r.t. it's rating, I_{SC} is increased

further. The variation in SPVE power output and grid power import and export are depicted in Table 2 and Fig. 13.
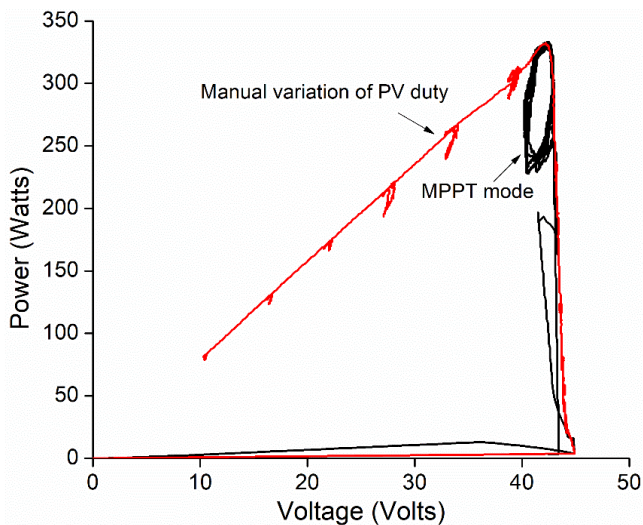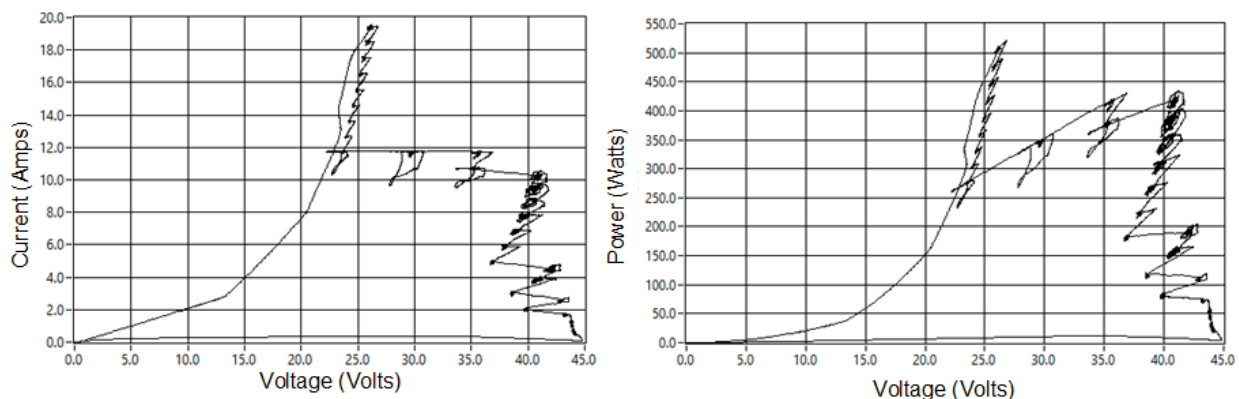

Fig. 12. P-V characteristics under MPPT

Fig. 13. I-V and P-V characteristics with a variation on PV duty and current rating

6. Conclusion

Renewable energy sources can fulfill the escalation in energy demand and sustainable development. Research and development improve the implementation plan of solar and wind energy plants throughout the world. In this paper, the various characteristics of the solar module have been presented using the hardware model of solar PV emulator and grid integrated DC microgrid. Overview of SPVE model, the study of I-V, P-V characteristics under variation of irradiation, and partial shading has been discussed. The grid integrated hardware model comprises solar emulator and LabVIEW-based GUI system for data acquisition has been used for experimental investigation under various conditions and module rating. With an increase in duty ratio of the buck converter, power produced from the emulator increases and starts exporting to the utility grid at 0.5. At converter duty near 0.65, the power generated from the solar module attains maximum value. The current reaches a maximum value while the voltage starts decreasing. The load line also shifts from the right side of the P-V curve to the left side. The graphical representation of MPPT tracking with a manual variation of duty ratio and MPPT controller helps the researcher differentiate between the two.

References

[1] BP, "BP Statistical Review of World Energy," 2020. Accessed: Dec. 15, 2020. [Online]. Available: https://www.bp.com/.

[2] M. S. Mahmoud and F. M. AL-Sunni, *Control and Optimization of Distributed Generation Systems.* Springer Berlin Heidelberg, 2015.

[3] G. Dileep and S. N. Singh, "Maximum power point tracking of solar photovoltaic system using modified perturbation and observation method," *Renewable and Sustainable Energy Reviews*, vol. 50. pp. 109–129, 2015, doi: 10.1016/j.rser.2015.04.072.

[4] G. K. Singh, "Solar power generation by PV (photovoltaic) technology: A review," *Energy*, vol. 53, pp. 1–13, 2013, doi: 10.1016/j.energy.2013.02.057.

[5] O. Bingöl and B. Özkaya, "Analysis and comparison of different PV array configurations under partial shading conditions," *Sol. Energy*, vol. 160, pp. 336–343, 2018, doi: 10.1016/j.solener.2017.12.004.

[6] H. Hanifi, M. Pander, B. Jaeckel, J. Schneider, A. Bakhtiari, and W. Maier, "A novel electrical approach to protect PV modules under various partial shading situations," *Sol. Energy*, vol. 193, no. July, pp. 814–819, 2019, doi: 10.1016/j.solener.2019.10.035.

[7] A. Mohapatra, B. Nayak, P. Das, and K. B. Mohanty, "A review on MPPT techniques of PV system under partial shading condition," *Renew. Sustain. Energy Rev.*, vol. 80, no. May, pp. 854–867, 2017, doi: 10.1016/j.rser.2017.05.083.

[8] G. Sai Krishna and T. Moger, "Reconfiguration strategies for reducing partial shading effects in photovoltaic arrays: State of the art," *Sol. Energy*, vol.

182, no. February, pp. 429–452, 2019, doi: 10.1016/j.solener.2019.02.057.

[9] I. Colak, R. Bayindir, and S. Sagiroglu, "The Effects of the Smart Grid System on the National Grids," in *8th International Conference on Smart Grid, icSmartGrid 2020*, 2020, pp. 122–126, doi: 10.1109/icSmartGrid49881.2020.9144891.

[10] V. Junior, F. Kakeu, A. T. Boum, and C. F. Mbey, "Optimal Reliability of a Smart Grid," *International Journal of Smart Grid*, vol. 5, no. 2, pp. 74–82, 2021.

[11] S. F. Jaber and A. M. Shakir, "Design and Simulation of a boost-Microinverter for Optimized Photovoltaic System Performance," *International Journal of Smart Grid*, vol. 5, no. 2, pp. 94–102, 2021.

[12] D. S. L. Dolan, J. Durago, and Taufik, "Development of a photovoltaic panel emulator using Labview," *Conf. Rec. IEEE Photovolt. Spec. Conf.*, pp. 001795–001800, 2011, doi: 10.1109/PVSC.2011.6186302.

[13] D. D. C. Lu and Q. N. Nguyen, "A photovoltaic panel emulator using a buck-boost DC/DC converter and a low cost micro-controller," *Sol. Energy*, vol. 86, no. 5, pp. 1477–1484, 2012, doi: 10.1016/j.solener.2012.02.008.

[14] J. P. Ram, H. Manghani, D. S. Pillai, T. S. Babu, M. Miyatake, and N. Rajasekar, "Analysis on solar PV emulators: A review," *Renew. Sustain. Energy Rev.*, vol. 81, no. May 2016, pp. 149–160, 2018, doi: 10.1016/j.rser.2017.07.039.

[15] V. Monteiro, T. J. C. Sousa, M. J. Sepulveda, C. Couto, A. Lima, and J. L. Afonso, "A Proposed Bidirectional Three-Level DC-DC Power Converter for Applications in Smart Grids: An Experimental Validation," in *SEST 2019 - 2nd International Conference on Smart Energy Systems and Technologies*, 2019, pp. 1–6, doi: 10.1109/SEST.2019.8849084.

[16] Y. Furukawa, H. Tomura, T. Suetsugu, and F. Kurokawa, "Variable feedback gain DC-DC converer tracing output voltage fluctuation for renewable energy system," in *8th International Conference on Renewable Energy Research and Applications, ICRERA 2019*, 2019, pp. 916–921, doi: 10.1109/ICRERA47325.2019.8996540.

[17] R. Ayop and C. W. Tan, "A comprehensive review on photovoltaic emulator," *Renew. Sustain. Energy Rev.*, vol. 80, no. May, pp. 430–452, 2017, doi: 10.1016/j.rser.2017.05.217.

[18] H. L. Tsai, "Insolation-oriented model of photovoltaic module using Matlab/Simulink," *Sol. Energy*, vol. 84, no. 7, pp. 1318–1326, 2010, doi: 10.1016/j.solener.2010.04.012.

[19] V. Lo Brano, A. Orioli, G. Ciulla, and A. Di Gangi, "An improved five-parameter model for photovoltaic modules," *Sol. Energy Mater. Sol. Cells*, vol. 94, no. 8, pp. 1358–1370, 2010, doi: 10.1016/j.solmat.2010.04.003.